Applications of Powder Densification Maps to Direct Metal SLS/HIP Processing

Martin Wohlert[†], David L. Bourell[†]*, Suman Das*, Joseph J. Beaman[†]*

[†]Texas Materials Institute
Laboratory for Freeform Fabrication
*Mechanical Engineering Department
University of Texas at Austin
Austin, TX 78712

Abstract

Recent investigations have shown that Direct Selective Laser Sintering in conjunction with Hot Isostatic Pressing (HIP) is capable of producing fully dense, near net shape, high performance metal components. A key aspect of this combined processing method is the selection of appropriate HIP process parameters to obtain full density parts. Powder Densification Maps provide a powerful tool for predicting the effect of time, temperature, pressure, and material properties on part density. This paper summarizes developments in Powder Densification Map production for Ti-6Al-4V and Inconel 625 materials. A comparison of theoretically predicted and experimentally determined densities for a variety of processing conditions is presented.

Introduction

The material densification rate during Hot Isostatic Pressing (HIP) is dependent on a variety of factors including: intrinsic material properties such as yield strength and diffusion rates; sample specific variables including the initial density, part geometry, and powder particle size; and HIP processing parameters such as temperature and pressure. The ability to model the densification process is beneficial and permits planning of more advanced process optimization such as control and modification of microstructure or geometric distortion.

The influence and interaction of the varying mechanisms exhibited across the entire processing envelope is most readily represented in a graphical format. This graphical representation has become known as a HIP map. The basis of this concept was developed by Weertman [1]; however, the construction of the maps was brought to fruition by Ashby [2] in the early 1970's. The constitutive equations for the generation of the maps have been incorporated into a computer program which was used to create the deformation maps provided here. In the following sections, the deformation mechanisms incorporated into the model and the accompanying constitutive equations will be reviewed. For two materials selected for SLS+HIP trials (Ti-6Al-4V and Alloy 625), material property data and calculated maps will be shown. Experimental data obtained from glass encapsulated HIP trials will be presented to validate the

HIP map results. A discussion of the accuracy of the theoretical predictions relative to the experimental results will be presented.

Powder Densification

The models developed for both conventional pressureless sintering and HIP assume an initial structure consisting of uniformly sized, perfectly spherical particles. This assumption greatly simplifies the calculations in comparison to a system of arbitrary, irregularly shaped particles, and in fact, is not too far removed from the powders selected for SLS+HIP. Initially the spherical particles are assumed to be in point contact as shown in Figure 1. As the sintering or HIP process proceeds, the contact area between particles increases to form "necks" or "bridges" between adjacent particles.

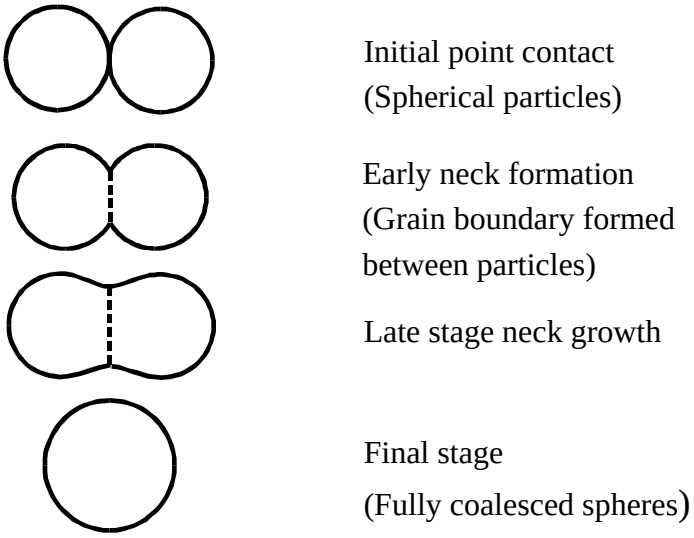

Figure 1. Model of sintering process for uniformly-sized, spherical particles (after German) [3]

In early stages of sintering, particle necks provide strength, but very little densification takes place. As sintering proceeds, necks continue to enlarge, and particles begin to coalesce, resulting in increasing bulk density. The enlarged necks between particles produce a cylindrical pore structure throughout the powder mass typified in Figure 2a. While this interconnected pore structure exists, it serves as an important conduit for mass transport; however, when a theoretical density of approximately 92% is reached, the continuous, cylindrical structure becomes unstable and collapses to form isolated spherical pores, as illustrated by black dots in Figure 2b. This transition is defined as the boundary between the initial sintering conditions, Stage I, and the later Stage II process. This change in sintering behavior requires a modification of the equations used to described the densification process. As a result, two different equations exist for each densification mechanism.

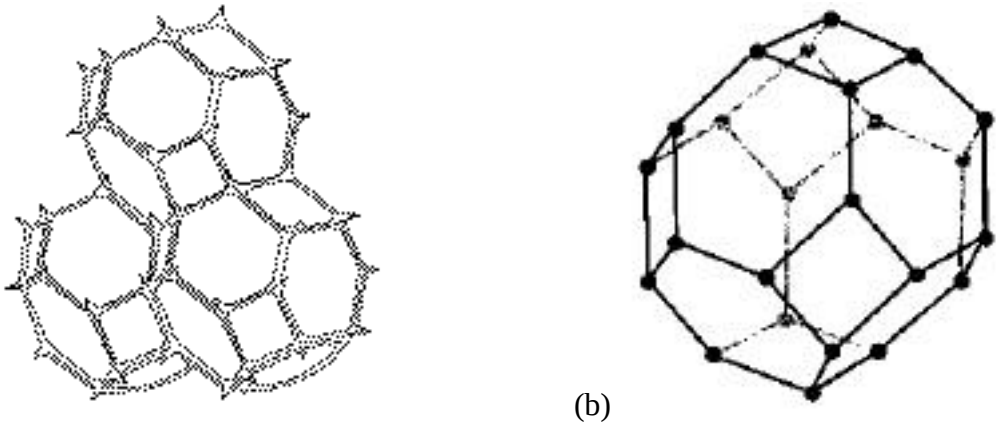

(a) (b)

Figure 2 Illustration of the (a) cylindrical Stage I pore structure and (b) isolated, spherical Stage II pore structure [4]

Driving Force for Densification

For pressureless sintering, a reduction in surface area is the only driving force for the densification of the powder mass. In the case of HIP, an additional driving force stemming from the stress created by the compaction pressure is also active. To provide a convenient and unified form of the two driving forces, the surface area component of the driving force is converted to an effective stress and summed with the net applied HIP gas pressure, as shown in Equations 1 and 2. A complete derivation of the equations is given by Ashby [5].

$$P_{total} = P_{ext} - P_0 + 3\Delta^2 \frac{\gamma}{R}\left(\frac{2\Delta - \Delta_o}{1 - \Delta_o}\right) \qquad \text{[Stage I]} \qquad (1)$$

$$P_{total} = P_{ext} - P_{int}\frac{(1-\Delta_c)\Delta}{(1-\Delta)\Delta_c} + 2\frac{\gamma}{R}\left(\frac{6\Delta}{1-\Delta}\right)^{\frac{1}{3}} \qquad \text{[Stage II]} \qquad (2)$$

where

P_{total} = Effective Applied Driving Pressure (Pa)
P_{ext} = HIP Pressure (Pa)
P_{int} = Internal Pore Pressure (Pa)
Δ = Relative Density = ρ/ρ_{th}
ρ = Part Density
ρ_{th} = Theoretical Density (g/cc)
γ = Powder Surface Energy (J/m^2)
R = Powder Radius (m)
Δ_o = Initial Relative Density

Δ_c = Relative Density at Pore Closure / Isolation

In practice, the contribution due to the surface energy reduction term is minor relative to realistic HIP pressures. A quick check using fairly typical values of R = 25 μm, γ = 2 J/m^2 indicates that even near the end of the densification process (Δ = 0.97), where the surface energy contribution is greatest, the effective pressure is still only 0.93 MPa. With typical HIP pressures on the order of 100 MPa, it is apparent that there is a substantial driving force increase associated with HIP compaction relative to conventional pressureless sintering.

Densification Mechanisms and Map Construction

In all stages of sintering, several densification mechanisms act simultaneously. In Ashby's initial analysis for pressure sintering maps, he included four independent mechanisms: lattice diffusion, grain boundary diffusion, power-law creep (or dislocation creep), and plasticity (yielding/dislocation glide). In more recent work, the additional mechanisms of Nabarro-Herring creep and Coble creep were included for cases where the internal grain size of the particles is substantially smaller than the particle diameter [6]. Grain growth and grain boundary separation from pores during Stage II densification are also incorporated into the model.

Having successfully defined constitutive equations for the densification mechanisms, calculation of the HIP maps may proceed. A flow chart of the process is shown in Figure 3. To begin the process, the values for all required material properties must be entered. Next, a starting temperature, pressure, and initial relative density Δ_o are set. The program calculates the densification rate contribution of each deformation mechanism and sums them to obtain an overall densification rate $\dot{\Delta}_{total}$. Then, an incremental increase in the relative density $\Delta\Delta$ is selected and the time (Δt) required to obtain the densification is calculated from $\Delta t = \Delta\Delta / \dot{\Delta}_{total}$. The dominant densification mechanism, the new relative density and the total elapsed time are recorded, and the entire process is repeated starting at the newly incremented density. Eventually, the relative density is incremented to the full theoretical density. At this point, a new temperature is selected, the relative density is reset to its initial value, and the entire process is repeated. The collected data is then used to generate a plot of relative density (Δ) versus temperature (T) for a given time in the form of isochronal lines. The information collected during each iteration on the dominant deformation mechanism may be indicated in appropriate regions on the map. A complete listing of the data used in constructing the HIP maps is given in the Table.

Experimental Verification of the HIP Model

The densification predictions of the HIP model were verified through a series of HIP experiments. Alloy 625 and Ti-6Al-4V powders were processed over a range of temperatures, pressures, and times. The density achieved for a particular set of processing conditions was

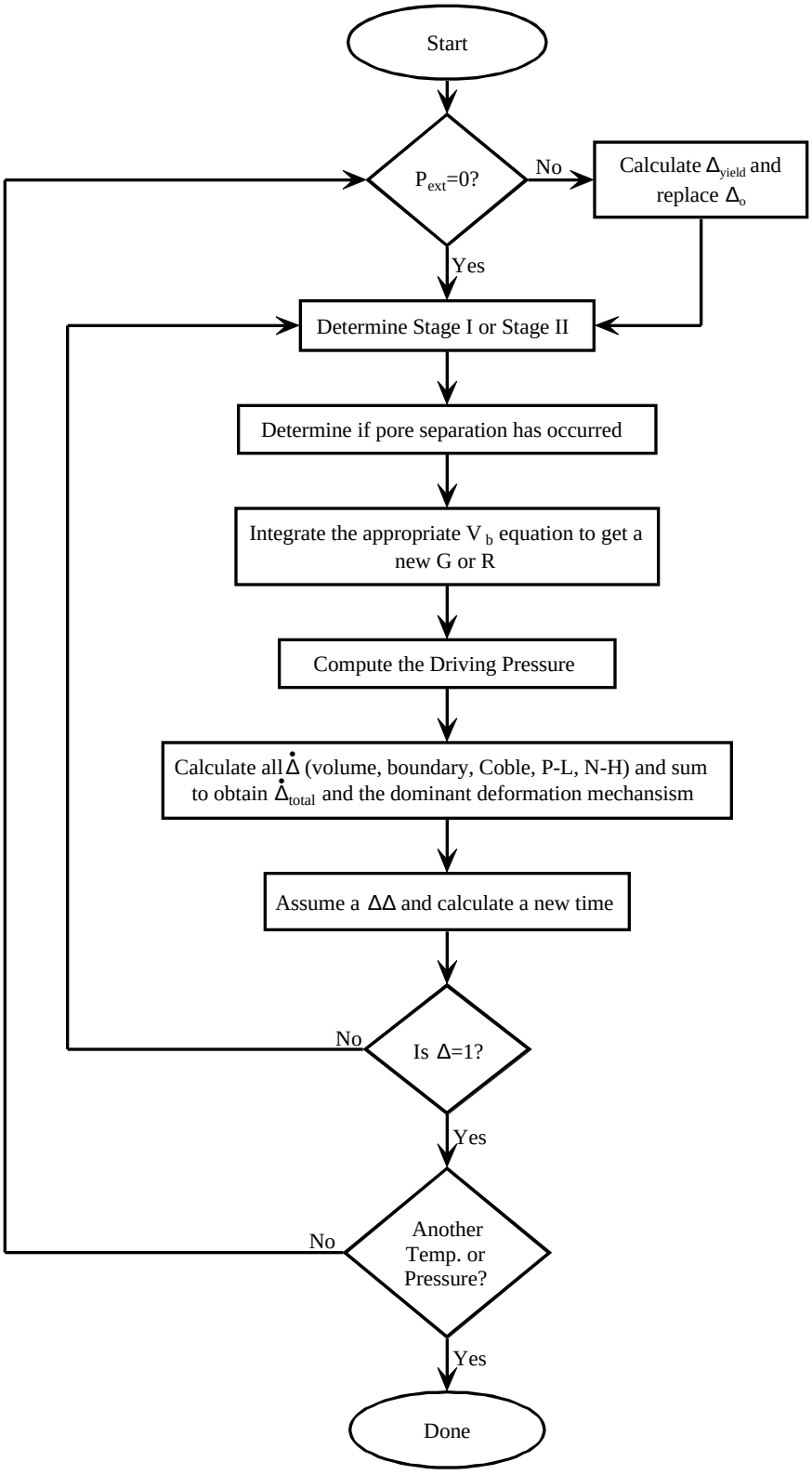

Figure 3 Generalized flowchart for a HIP Sintering model program

Table - Material Property Values for HIP Map Calculations

Variable	Symbol	Alloy 625	Ti-6Al-4V
Melting Temperature	T_m	1563 K	1877 K
Theoretical Density	ρ	8.44 g/cc	4.43 g/cc
Compact Initial Density	ρ_{th}	0.60	0.60
Particle Size (radius)	R	$25x10^{-6}$ m	$27.5x10^{-6}$ m
Initial Grain Size	-	$5x10^{-6}$ m	$1x10^{-6}$ m
Grain Size Ratio	-	0.33	0.5
Surface Diffusion Pre-exponential	D_s	$2.1x10^{-4}$ m^2/s	1000 m^2/s
Surface Diffusion Activation Energy	Q_s	163 J/mol	150 kJ/mol
Grain Boundary Mobility Pre-exponential	D_{GBM}	$8.53x10^{-6}$ m^2/s	1.24e-4 m^2/s
Grain Boundary Mobility Activation Energy	Q_{GBM}	290 J/mol	104 kJ/mol
Surface Free Energy	γ	1.96 J/m^2	2.3 J/m^2
Yield Strength at Room Temp.	σ_{ys}	490 MPa	875 MPa
Linear temp. dependence of Y.S.	-	0.02 MPa/K	0.82 MPa/K
Atomic Volume	Ω	$1.09x10^{-29}$ m^3	$1.76x10^{-29}$ m^3
Power Law Creep Exponent	n	8	2
Power Law Creep Activation Energy	Q_c	269 kJ/mol	225
Power Law Creep Reference Stress	σ_{ref}	900 MPa	100 M Pa
Volume Diffusion Pre-exponential	D_V	$1.2x10^{-3}$ m^2/s	$6.6x10^{-9}$ m^2/s
Volume Diffusion Activation Energy	Q_V	259 kJ/mol	169 kJ/mol
Boundary Diffusion Pre-exponential	D_B	$7.17x10^{-3}$ m^2/s	$1.2x10^{-5}$ m^2/s
Boundary Diffusion Activation Energy	Q_B	209 kJ/mol	97 kJ/mol
Grain Boundary Width	δ	$6x10^{-10}$ m	$6x10^{-10}$ m

measured by gas pycnometry or Archimedes' principle and compared to the value predicted by the HIP maps. Powder was placed in borosilicate glass, evacuated to at least $5x10^{-5}$ Torr, degassed at 350°C for a minimum of 24 hours to remove the majority of surface adsorbed gases as well as some species dissolved within the powder [7], and the glass tube was sealed prior to HIP. The glass capsules were processed in an ABB QIH-3 HIP system equipped with a graphite heating element. The process cycle began with a 10°C/min ramp from room temperature to the

desired processing temperature. Once the operating temperature was reached, the pressure within the HIP vessel was raised. After the desired processing time had elapsed, the temperature was decreased at 15°C/min and the pressure was gradually reduced to atmospheric pressure.

Results and Discussion

A HIP map was generated for the Alloy 625 material as shown in Figure 4. All three operating parameters (time, temperature, and pressure) were varied in the HIP experiments. In most cases, the predicted values are within one or two percent of the experimentally determined density.

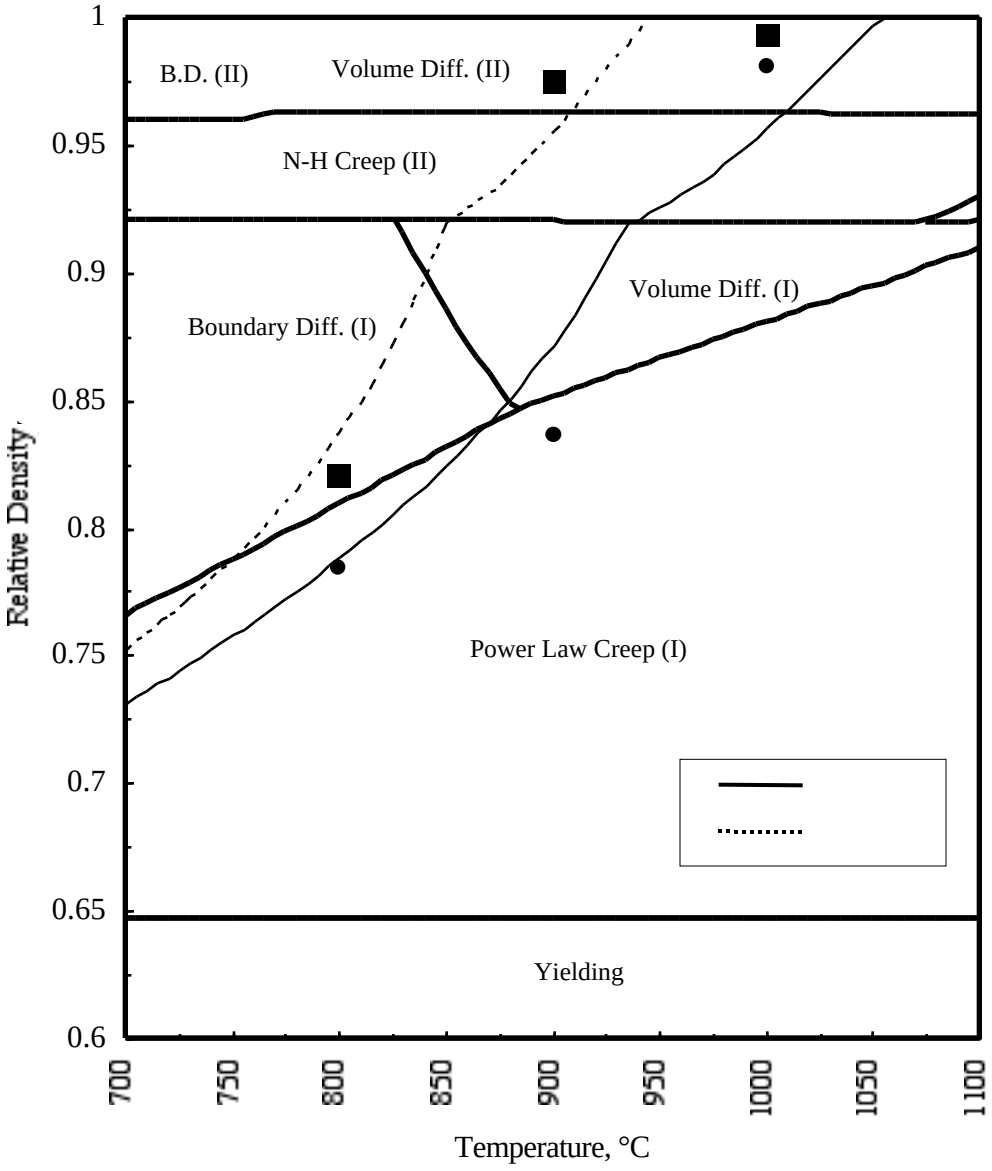

Figure 4 HIP map for Alloy 625. HIP pressure = 10 ksi. Experimentally determined values have been plotted for 1 hour (●) and 8 hours (■).

A similar set of experiments and HIP maps were generated for the Ti-6Al-4V material. The results are shown in Figure 5. The short process cycle data (5 min) still show significant deviation from the theoretical values. It has been clearly demonstrated by a number of researchers that fine grained (<10 μm) Ti-6Al-4V exhibits superplastic behavior at temperatures near 900°C [8,9]. These authors have suggested that a grain boundary sliding (GBS) mechanism accounts for the behavior of the material under the specified processing conditions. This mechanism is currently not included in the HIP Map model. A number of constitutive relationships have been developed to describe deformation associated with grain boundary sliding (or shearing). The incorporation of an appropriate rate equation into the model could improve the prediction accuracy for superplastic materials such as Ti-6Al-4V.

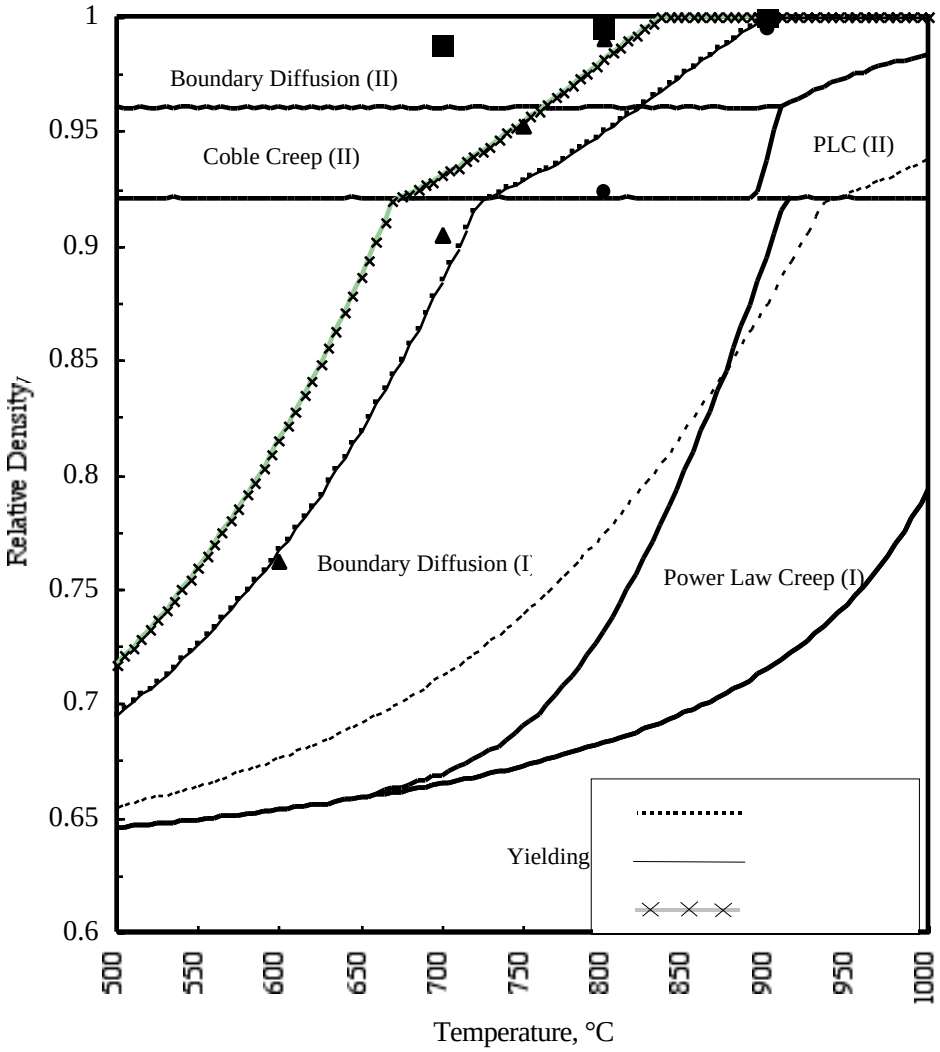

Figure 5 HIP Map for Ti-6Al-4V. HIP pressure = 10 ksi. Experimentally determined values have been plotted for 0.1 hour (●), 2 hours (▲), and 4 hours (■).

Summary and Conclusions

HIP maps were generated to predict the densification behavior of Alloy 625 and Ti-6Al-4V. The ability to accurately determine an appropriate HIP cycle without substantial trial-and-error testing could greatly reduce the time and cost associated with the development of SLS+HIP processes for new materials. The HIP maps were constructed by calculating the densification contributions of several independent deformation mechanisms: lattice diffusion, boundary diffusion, power-law creep, Nabarro-Herring creep, and Coble creep. The density predictions of the HIP map model were verified by experimental HIP cycles run on glass encapsulated powders.

In general, the results of the Alloy 625 and Ti-6Al-4V modeling are quite illustrative of the benefits and limitations of the mechanistic model approach. As was demonstrated, the model typically provides a useful qualitative description of the densification rate without requiring a high degree of accuracy in the material property data. The quantitative results, however, are highly dependent on the material property data selected for the model. For most materials it is found that power law creep dominates the densification process over a wide range of processing conditions. Boundary diffusion provides a substantial supporting role, particularly at moderate temperatures. This suggests that densification rates at moderate processing temperatures may be highly dependent on particle size. Additional experiments, measuring the effect of particle size variations on densification rate could be useful to further verify the accuracy of the HIP maps.

References

[1] Weertman, Trans Met. Soc AIME. 227,1475 (1963).

[2] M. F. Ashby, "A first Report on Deformation-Mechanism Maps," *Acta Metallurgica,* Vol. 20 (1972) pp. 887-897.

[3] Randall M. German, *Powder Metallurgy Science*, *Second Edition*. Metal Powder Industries Federation, Princeton, NJ, (1994), p.245.

[4] Ibid., pp.254-5.

[5] M.F. Ashby, *Sintering and Isostatic Pressing Diagrams*, Published by Author, Department of Engineering Cambridge, England (1990).

[6] A.S. Helle, K.E. Easterling, and M.F. Ashby, *Acta Metall.* Vol.33 No. 12 (1985) pp.2163-2174.

[7] B. Engel, "Preprocessing of Ti-6Al-4V powder for applications in Selective Laser Sintering/Hot Isostatic Pressing (SLS/HIP)," Master's Thesis, The University of Texas at Austin, (1998).

[8] A.K. Ghosh and C.H. Hamilton, *Met. Trans. A,* Vol. 10A, (1979) pp. 699-706.

[9] N.E. Paton and C.H. Hamilton, *Met. Trans.s A,* Vol. 10A, Feb. 1979, pp.241-250.